ACS central science

Research Article

http://pubs.acs.org/journal/acscii

Combating Drug-Resistant Mutants of Anaplastic Lymphoma Kinase with Potent and Selective Type-I$^{1/2}$ Inhibitors by Stabilizing Unique DFG-Shifted Loop Conformation

Peichen Pan,[†] Huidong Yu,[‖] Qinglan Liu,[§,▽] Xiaotian Kong,[†,⊥] Hu Chen,[§] Jiean Chen,[§] Qi Liu,[§] Dan Li,[†] Yu Kang,[†] Huiyong Sun,[†] Wenfang Zhou,[†] Sheng Tian,[#] Sunliang Cui,[†] Feng Zhu,[†] Youyong Li,[⊥] Yong Huang,[*,§] and Tingjun Hou[*,†,‡]

[†]College of Pharmaceutical Sciences and [‡]State Key Lab of CAD&CG, Zhejiang University, Hangzhou, Zhejiang 310058, China

[§]Key Laboratory of Chemical Genomics, School of Chemical Biology and Biotechnology, Shenzhen Graduate School, Peking University, Shenzhen, Guangdong 518055, China

[‖]Rongene Pharma Co., Ltd., Shenzhen, Guandong 518054, China

[⊥]Institute of Functional Nano and Soft Materials (FUNSOM) and [#]Jiangsu Key Laboratory of Translational Research and Therapy for Neuropsychiatric Diseases and College of Pharmaceutical Sciences, Soochow University, Suzhou, Jiangsu 215123, China

[▽]Innovative Drug R & D Center, Shenzhen Salubris Pharmaceuticals Co., Ltd., Huabao Industrial Zone, Shenzhen 518102, China

S *Supporting Information*

ABSTRACT: Targeted inhibition of anaplastic lymphoma kinase (ALK) dramatically improved therapeutic outcomes in the treatment of ALK-positive cancers, but unfortunately patients invariably progressed due to acquired resistance mutations in ALK. Currently available drugs are all type-I inhibitors bound to the ATP-binding pocket and are most likely to be resistant in patients harboring genetic mutations surrounding the ATP pocket. To overcome drug resistance, we rationally designed a novel kind of "bridge" inhibitor, which specially bind into an extended hydrophobic back pocket adjacent to the ATP-binding site of ALK. The novel type-I$^{1/2}$ inhibitors display excellent antiproliferation activity against ALK-positive cancer cells and appear superior to two clinically used drugs, crizotinib and ceritinib. Structural and molecular modeling analyses indicate that the inhibitor induces dramatic conformational transition and stabilizes unique DFG-shifted loop conformation, enabling persistent sensitivity to different genetic mutations in ALK. These data highlight a rationale for further development of next-generation ALK inhibitors to combat drug resistance.

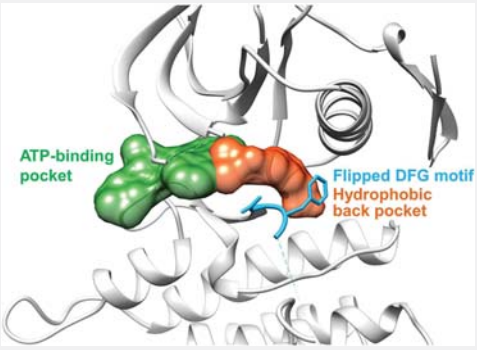

INTRODUCTION

As the first approved anaplastic lymphoma kinase (ALK) inhibitor by the U.S. Food and Drug Administration (FDA) in 2011, crizotinib (Xalkori) has become a prescription medicine used to treat people with ALK$^+$ or ROS1$^+$ metastatic nonsmall cell lung cancer (NSCLC).[1,2] Most NSCLC patients harboring ALK were highly sensitive to crizotinib, but unfortunately tumors invariably progressed after 1−2 years of treatment due to the emergence of drug resistance.[3] Point mutations within the ALK kinase domain have been identified in approximately 1/3 of crizotinib-resistant patients.[4,5] In 2010, two secondary mutations within the kinase domain of EML4-ALK (the most frequent gatekeeper mutation L1196M and mutation C1156Y) were discovered in a patient during the relapse phase of treatment with crizotinib,[6] and thereafter, various resistant mutations were identified, such as F1174L, G1269A, G1202R, S1206Y, L1152R, and insertion mutation 1151Tins.[4,7−10] In addition to the influence of ALK mutations on acquired drug resistance, some ALK mutants (e.g., R1275Q and F1174L) are stably expressed in a number of cancer cell lines and directly initiate tumor formation by regulating MYC expression in oncogenic process.[11] Thus, there is an urgent need to discover and design new chemical entities that could inhibit various ALK mutants.

Some efforts have been made to develop new inhibitors of ALK to combat drug resistance, but few inhibitors can potently inhibit the broad range of ALK mutants. Ceritinib (LDK-378) is the second FDA-approved inhibitor of ALK and can effectively inhibit several crizotinib-resistant mutations (e.g., L1196M and G1269A), but it cannot overcome some other resistant ALK mutants, including G1202R and F1174C.[12,13] In late 2015, alectinib was approved under the FDA's accelerated approval program, and it can overcome several known

Received: September 9, 2017
Published: November 3, 2017

DOI: 10.1021/acscentsci.7b00419
ACS Cent. Sci. 2017, 3, 1208−1220

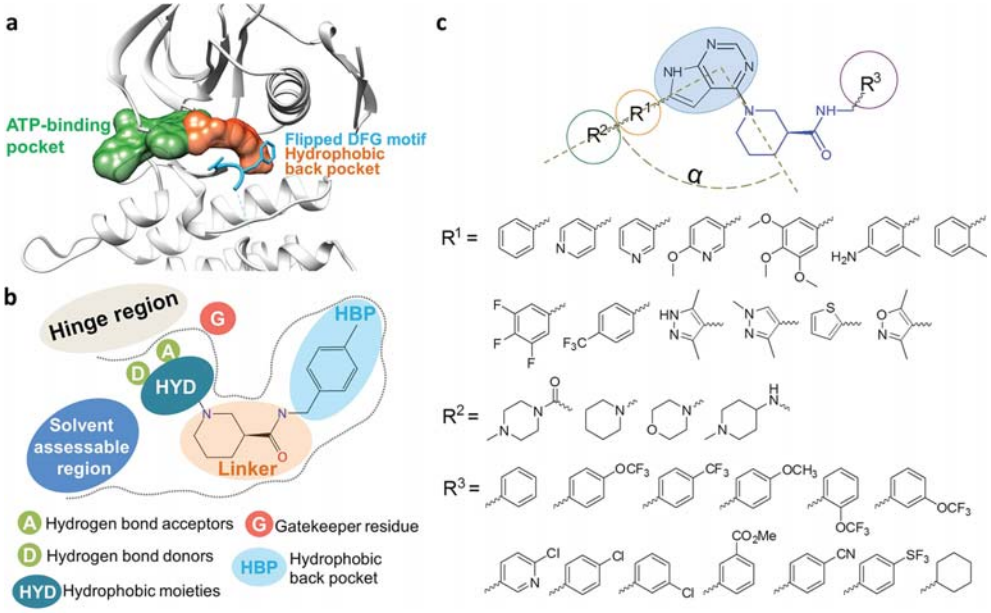

Figure 1. Rational design of possible "bridge molecules" that could target both ATP-binding site and back pocket. (a) Representation of the binding pocket of ALK. Protein structure is shown in gray ribbon. The ATP-binding pocket is colored in green, and the hydrophobic back pocket is colored in orange. The structure of the shifted DFG motif is highlighted and shown in cyan. (b) Schematic illustration of the potential pharmacophore representing the interactions in the hinge region and hydrophobic back pocket. Part of the piperidine carboxamide structure that locates in the linker region and the deep back pocket is displayed and highlighted. Hydrogen bond donor and acceptor are shown by the green circles labeled D and A, respectively. The circle labeled HYD represents the hydrophobic moiety that occupies the adenine ring region. (c) Rational design of type-$I^{1/2}$ inhibitors. Various building structures substituted in different regions are also listed.

mutations but is also inactive against other mutations, such as G1202R, I1171, and F1174V.[14,15] Similarly, other ALK inhibitors also exhibit inconstant potency against various resistant mutants of ALK.[16] On April 28, 2017, FDA granted accelerated approval to brigatinib,[17] which is also classified as a second-generation inhibitor and cannot cover the broad range of drug-resistant mutations either. The results from phase II trial enrolling 222 crizotinib-resistant patients showed that the overall response rate (ORR) of two different dose strategies was 45% and 55%, respectively.[18] Brigatinib is now in both phase III first-line setting and phase II study with patients resistant to ceritinib and alectinib. Besides, several other ALK inhibitors are currently under clinical assessment, such as lorlatinib (Phase I/II, Pfizer),[19] entrectinib (Phase II, Ignyta),[20] and ensartinib (Phase II, Xcovery).[21] Lorlatinib is a highly activity ALK inhibitor with IC_{50} lower than 0.07 nM and can block most mutations resistant to crizotinib, ceritinib, and alectinib. In a phase I/II trial on 43 patients, the ORR of lorlatinib was 46% with or without treatment of prior ALK inhibitors.[22] Entrectinib can target both ALK and NTRK1−3 fusion protein. In a phase I study enrolling 24 patients without treatment with other ALK inhibitors, the ORR of entrectinib was 57%, 100%, and 85% for ALK^+, $NRTK1-3^+$, and $ROS1^+$ patients, respectively.[23] Remarkably, the ORR of ensartinib (X-396) in a phase I study enrolling 52 resistant patients was 88% by serial plasma sequencing that helps to select specific patients.[24]

Currently available drugs and candidates in ongoing clinical trials are all type-I inhibitors bound to the ATP-binding pocket of ALK (Figure 1a) in its active DFG (Asp-Phe-Gly)-in state, and thus are most likely to be ineffective in patients harboring genetic mutations surrounding the ATP pocket (e.g., L1196M, G1202R, G1269A, and S1206Y), which are the main cause of drug resistance observed in clinic. In contrast, there exists another kind of inhibitor, so-called type-II or type-$I^{1/2}$ inhibitors, occupying an extended hydrophobic tunnel (see in Figure 1a) adjacent to the ATP-binding site, which could induce a distinct DFG-out or DFG-shifted loop conformation. These compounds show several advantages over the type-I inhibitors, such as improved kinase selectivity, slower off-rates with extended residence time,[25] and coverage of broad ALK mutations. So far, only a few type-II or type-$I^{1/2}$ inhibitors of ALK have been identified, and the potency of these molecules is generally weak,[26,27] thus hindering further development.

We hypothesized that designing a new scaffold that bridges both the ATP-binding pocket and the hydrophobic back pocket might be an effective way to identify a potent type $I^{1/2}$ inhibitor with improved ligand binding affinity toward both wild-type and drug-resistant mutants of ALK, as well as kinase selectivity to avoid potential off-target effects. In the present work, a series of novel type-$I^{1/2}$ inhibitors were rationally designed and synthesized, and the experimental results demonstrate that these compounds show potent inhibitory activity in *in vitro* ALK enzyme-based assay and superior antiproliferation activity in three ALK-positive cancer cell lines (NCI-H2228, NCI-H3122, and Karpass-299), when compared to the two clinically used drugs, crizotinib and ceritinib. Furthermore, the sensitivity of compound **001**-**017** against four resistant ALK mutants was also found to be better than those of both crizotinib and ceritinib. Structural and molecular modeling analyses indicate that the inhibitor induces dramatic conformational transition and stabilizes unique DFG-shifted loop conformation enabling persistent sensitivity to different resistant mutations in ALK.

DOI: 10.1021/acscentsci.7b00419
ACS Cent. Sci. 2017, 3, 1208−1220

Table 1. ALK Kinase Inhibitory Activity (IC_{50}) for Compound 001-001−001-13 with R^1 Substitutions

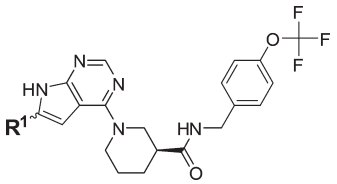

Compound	R_1	IC_{50}, nM (± SD) [a]	Compound	R_1	IC_{50}, nM (± SD) [a]
Crizotinib	---	4.66 (± 0.53)	**001-007**	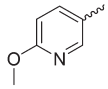	148.15 (± 9.88)
LDK-378 (Ceritinib)	---	3.94 (± 0.21)	**001-008**		11.48 (± 1.01)
001-001		52.47 (± 3.78)	**001-009**		6.01 (± 0.53)
001-002	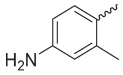	5.34 (± 0.27)	**001-010**	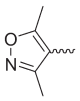	18.85 (± 0.79)
001-003	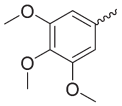	81.97 (± 5.18)	**001-011**	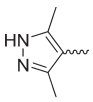	1.25 (± 0.09)
001-004	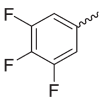	> 2000	**001-012**		3.7 (± 0.14)
001-005	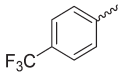	> 2000	**001-013**		37.88 (± 4.33)
001-006		11.88 (± 0.94)			

[a]All values are the average of $n \geq 2$ ± standard deviation.

RESULTS AND DISCUSSION

Rational Design of Type-$I^{1/2}$ Inhibitors of ALK Targeting Both ATP-Binding Site and Additional Hydrophobic Back Pocket. Type-$I^{1/2}$ inhibitors are a novel class of kinase inhibitors that target the back pocket of ATP in either catalytically active or inactive DFG-in loop state, and can be recognized as a hybrid of type-I and type-II inhibitors.[28] The back pocket is typically hydrophobic with its size and shape regulated by the type of gatekeeper residue, and the cavity cannot be occupied by ATP. Piperidine carboxamide 1 (see in Figure 3e), which binds into the extended hydrophobic back pocket, was first reported as an ALK inhibitor by Bryan and co-workers in 2012,[26] and is at present the only type-$I^{1/2}$ inhibitor of ALK. However, the binding affinity of piperidine carboxamide 1 is relatively weak (inhibitory IC_{50} = 0.174 μM in ALK enzyme-based assay), and there is no relevant cellular data reported so far. In our previous study, the binding features of piperidine carboxamides were comprehensively analyzed by using combined molecular modeling strategies.[29] We observed that piperidine carboxamides can form strong interactions with the residues surrounding the hydrophobic back pocket, but lack favorable contacts with the residues in the ATP-binding site. Thus, in the present work, part of the piperidine carboxamide structure which binds to the linker region and the hydrophobic back pocket of ALK (see in Figure 1b) is harnessed as a chemical probe to build "bridge molecules" that could occupy both the ATP-binding site and the hydrophobic back pocket.

Type-I inhibitors bind to the ATP-binding pocket and typically recognize the active DFG-in loop conformation of the target. Generally they mimic the adenine moiety of ATP and fit into the ATP pocket by forming hydrogen bond interactions with the backbone atoms of the corresponding residues in the hinge region as well as establishing hydrophobic contacts in the adenine-binding region. Therefore, in order to construct a similar pharmacophore containing hydrogen bond donors and/or acceptors and hydrophobic moieties, pyrrole pyrimidine, with a rigid conjugate structure, was proposed and tethered to the starting piperidine carboxamide structure (Figure 1c). Molecular modeling study indicates that two hydrogen bonds can be formed between the residue Met1199 and the nitrogen atoms of pyrrole pyrimidine, which can well mimic the hydrogen bonds with the adenine moiety. The R^1 region also

DOI: 10.1021/acscentsci.7b00419
ACS Cent. Sci. 2017, 3, 1208−1220

Table 2. ALK Kinase Inhibitory Activity (IC_{50}) for Compound 001-014–001-17 with R^2 and R^4 Substitutions

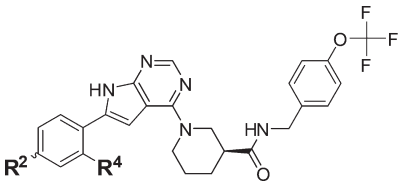

Compound	R_2	R_4	IC_{50}, nM (±SD) [a]
001-014	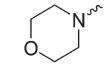	-H	11.2 (± 2.31)
001-015	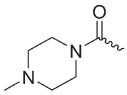	-H	0.6 (± 0.04)
001-016		-methyl	20.25 (± 0.97)
001-017	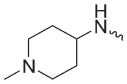	-methyl	0.27 (± 0.03)

[a]All values are the average of $n \geq 2$ ± standard deviation.

resides in a relatively hydrophobic environment between the adenine-binding region and the solvent accessible region. According to previous studies of type-I inhibitors, a phenyl ring which typically forms hydrophobic interactions with the glycine-rich loop residue Leu1122 is a choice of high priority and therefore was introduced to pyrrole pyrimidine at position **1** to optimally induce a $\alpha = 90–110°$ angle change (Figure 1c). In addition, compounds with different substitutions on the phenyl ring and various heterocyclic groups were also designed and synthesized. The R^2 moiety at the *para*-position of R^1 protrudes into the solvent accessible region and was replaced by several basic amine-containing solubilizing groups. With respect to the hydrophobic R^3 region, various functional groups, such as trifluoromethoxy, trifluoromethyl, methoxy, cyano and chloro groups, were designed and replaced at the *ortho*-, *meta*-, and *para*-position of the phenyl ring for better binding.

Inhibitory Potency in Biochemical Assay and Structure–Activity Relationship (SAR) Studies. To evaluate the inhibitory activity against ALK in *in vitro* models, time-resolved fluorescence resonance energy transfer (TR-FRET) assays were carried out for all the synthesized compounds as well as two positive control drugs, crizotinib and ceritinib. The IC_{50} value of each compound was determined from the fitted dose–response curve, and the data are summarized in Table 1 to Table 3. Initially, we replaced the R^1 moiety with a substituted phenyl ring and R^3 with a *para*-trifluoromethylphenyl group, leading to analogue **001-001**. The inhibitory IC_{50} value of this compound is 52.47 nM, which is about 3-fold more potent than that of piperidine carboxamide 1 (IC_{50} = 174 nM). This result confirms the effectiveness of using a phenyl ring at R^1, and, at the same time, demonstrates the feasibility of applying the pyrrole pyrimidine scaffold as a binder to the adenine-binding region. Modifications of the phenyl group with different substituents, including methoxyl, trifluoromethyl, amino and fluorine, yielded compounds **001-002** to **001-005**. It was observed that a methoxyl group at the *meta*- or *para*-position of the phenyl ring leads to slightly reduced inhibitory activity, and a fluorine or trifluoromethyl group significantly worsens IC_{50}. In sharp contrast, compound **001-002** with a more hydrophilic amino group substituted at the *para*-position exhibits noticeably improved activity (IC_{50} = 5.34 nM), a ∼10-fold increase relative to that of **001-001**. By replacing the phenyl ring with a more hydrophilic pyridine ring at R^1, both compounds **001-006** and **001-008** show improved activity. The tethering position of the pyridine has little influence on the activity. Compound **001-007** with a methoxyl group substituted at the *para*-position of the pyridine ring shows a 10-fold decrease in activity compared with **001-006**. Besides pyridine, five-membered heterocycles were also examined. We are pleased to find that the IC_{50} values of the responding analogues (**001-009**, **001-0011**, and **001-012**) are all less than 10 nM.

During the first round of optimization, the *para*-position (R^2) of the left phenyl group seems very sensitive to structural changes. We decided to fine-tune R^2 in the next phase (Table 2), which directly protrudes into the solvent accessible region. Several hydrophilic nitrogen-containing solubilizing groups were examined. Compounds **001-015** and **001-017** show excellent inhibitory potency with IC_{50} values in the picomolar range, 0.6 nM and 0.27 nM, respectively. Under the same assay conditions, the IC_{50} readouts of crizotinib and ceritinib are 4.66 nM and 3.94 nM, respectively. In comparison, **001-017** is substantially more potent than both marketed drugs.

Optimization was also carried out for the moiety that sits in the deep hydrophobic back pocket (phenyl group on the right, R^3) (see in Table 3). This phenyl group was substituted with various functionalities. Compound **002-004** without any substituent on the phenyl ring exhibits ∼100-fold decreased activity relative to **001-017**, demonstrating the importance of having a trifluoromethoxy moiety at the *para*-position. Substitution of the trifluoromethoxy group at the *ortho*-position of the R^3 phenyl (**002-003**) has a negative effect with IC_{50} = 61.12 nM. Trifluoromethoxylation at the *meta*-position results in a potent analogue **002-008** (IC_{50} = 0.64 nM). Replacing the trifluoromethoxy group by other groups, including trifluoromethyl, methylsulfonyl, sulfur trifluoride, methoxy, cyano and

DOI: 10.1021/acscentsci.7b00419
ACS Cent. Sci. 2017, 3, 1208–1220

Table 3. ALK Kinase Inhibitory Activity (IC_{50}) for Compound 002-001−002-17 with R^3 Substitutions

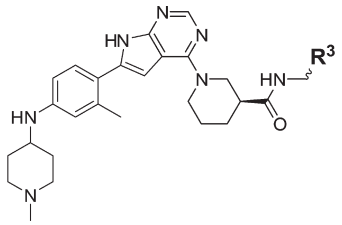

Compound	R_3	IC_{50}, nM (± SD) [a]	Compound	R_3	IC_{50}, nM (± SD) [a]
002-001	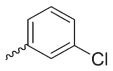	3.15 (± 0.45)	**002-010**	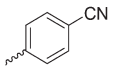	3.38 (± 0.32)
002-002	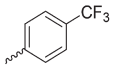	1.65 (± 0.79)	**002-011**	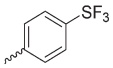	0.6 (± 0.07)
002-003		61.12 (± 3.22)	**002-012**	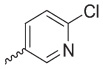	291.38 (± 6.87)
002-004		24.18 (± 1.02)	**002-013**		358.62 (± 12.34)
002-005	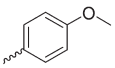	2.99 (± 0.16)	**002-014**	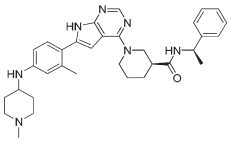	39.87 (± 2.23)
002-006	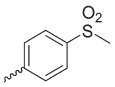	347.52 (± 7.64)	**002-015**	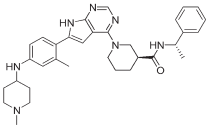	159.5 (± 7.33)
002-007		0.86 (± 0.13)	**002-016**	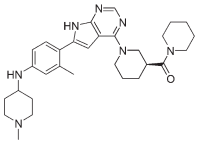	1921.69 (± 14.59)
002-008	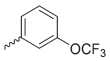	0.64 (± 0.07)	**002-017**	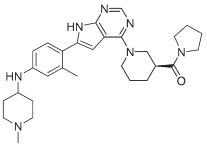	1205.98 (± 9.12)
002-009		2.18 (± 0.18)			

[a]All values are the average of $n \geq 2$ ± standard deviation.

chloro groups, all lead to weaker inhibitors. For example, analogue **002-006** with a hydrophilic methylsulfonyl group has an IC_{50} value of 347.52 nM. This observation validates the fact that the back pocket is primarily surrounded by hydrophobic amino acids, so the interactions between inhibitors and protein in this region should be predominantly hydrophobic. The importance of the R^3 phenyl was further confirmed by replacing it with other rings, such as pyridine, cyclohexane, or smaller saturated heterocyclic groups (**002-012**, **002-013**, **002-016**, and **002-017**). Weak inhibition was generally obtained, with the IC_{50} values ranging from 291.38 nM to 1921.69 nM.

Superior Cellular Activity against NSCLC and ALCL Cell Lines. The analogues were assessed for their bioactivities to inhibit the proliferation of ALK-positive cancer cells, including two NSCLC cell lines expressing EML4-ALK fusion (NCI-H2228 and NCI-H3122) and an ALCL cell line Karpas-299 with NPM-ALK fusion. Serial dilutions from 5000 ng/mL to 1.6 ng/mL were tested for each inhibitor, and the cell viability was determined by the MTT assay. The experimental results for several representative inhibitors are summarized in Figure 2, and the full cellular data for all the compounds can be found in Supplementary Table S1. As we can see in Figure 2b, at high concentrations all compounds show good inhibitory activities against NCI-H2228, while at low concentrations significant divergence is observed. The inflection point of the activity appears at the concentration of 40 ng/mL, and the differences become greater at 8 ng/mL where the inhibition ratios of cirizotinib and ceritinib drop sharply to 20.59% and 36.57%, respectively. At this concentration, compounds **001-017** and **002-008** give 71.67% and 63.08% inhibition of cell

DOI: 10.1021/acscentsci.7b00419
ACS Cent. Sci. 2017, 3, 1208−1220

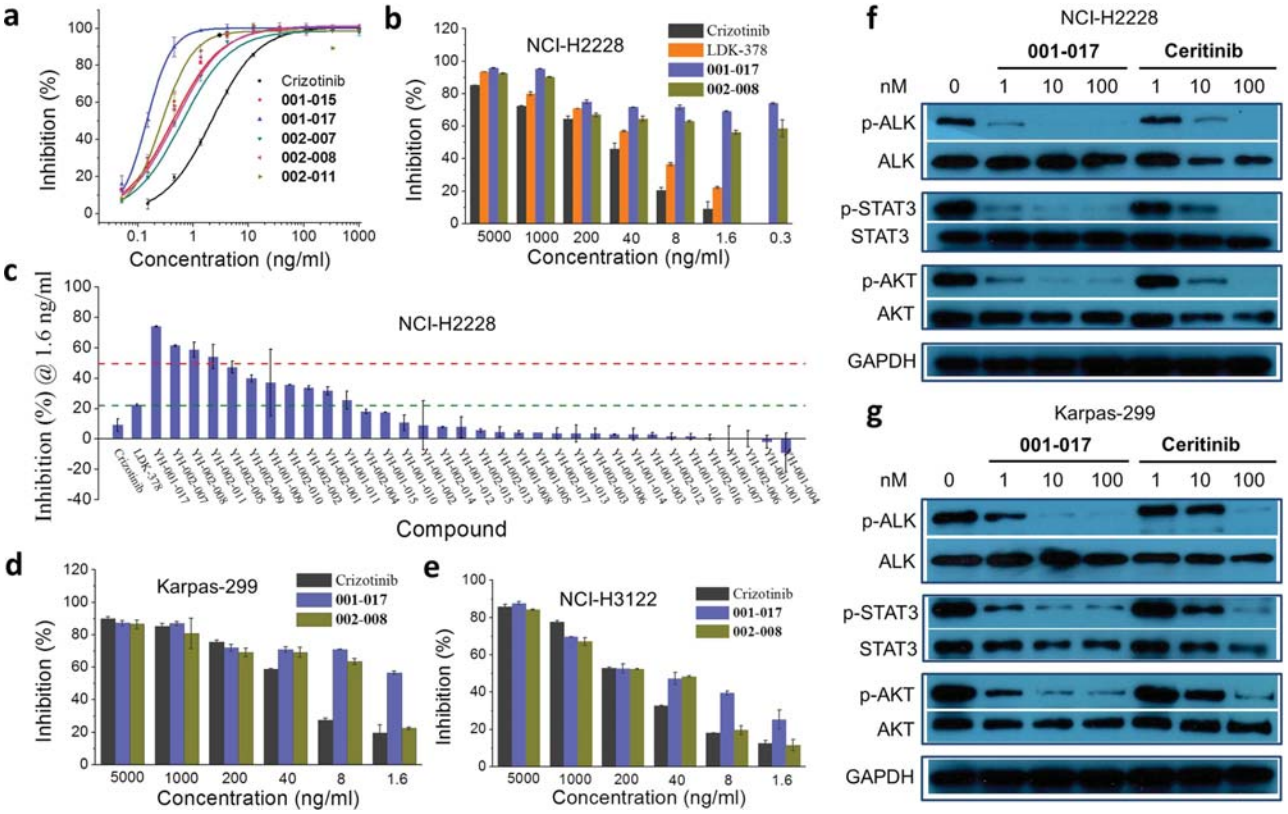

Figure 2. Inhibitory activities of the synthesized type-I$^{1/2}$ inhibitors. (a) Enzyme-based activities of several representative compounds against wild-type ALK. The resulting activities calculated from TR-FRET emission ratios are plotted against compound concentrations, and the dose−response curves are then fitted and plotted with variable slops. All values are the average of $n \geq 2 \pm$ standard deviation. (b) Antiproliferation activity of representative compounds against NSCLC cell line NCI-H2228. Cell viability is determined by MTT assay. (c) Inhibitory activities of all the synthesized compounds against NCI-H2228 at the concentration of 1.6 ng/mL. (d) Antiproliferation activity of representative compounds against ALCL cell line Karpas-299. (e) Antiproliferation activity of representative compounds against NSCLC cell line NCI-H3122. (f) Inhibition of ALK phosphorylation and downstream signaling pathways in H2228 cell line. Cells were treated with compounds for 2 h at indicated concentrations. ALK, Phospho-ALK, AKT, Phospho-AKT, STAT3, and Phospho-STAT3 were detected by immunoblot analysis using antibodies specific to each of them. (g) Inhibition of ALK phosphorylation and downstream signaling pathways in Karpas-299 cell line. Cells were treated with compounds for 2 h at indicated concentrations. ALK, Phospho-ALK, AKT, Phospho-AKT, STAT3, and Phospho-STAT3 were detected by immunoblot analysis using antibodies specific to each of them.

viability. When tested at the concentration of 1.6 ng/mL, cirizotinib and ceritinib show no inhibition, while **001-017** and **002-008** deliver remarkable results, 69.09% and 56.16% inhibition. These results indicate that **001-017** and **002-008** are excellent antiproliferation inhibitors against NCI-H2228, which are superior to both cirizotinib and ceritinib.

We further examined the inhibitory activities of all the synthesized compounds against NCI-H2228 at the lowest concentration of 1.6 ng/mL (shown in Figure 2c). Ten compounds show higher inhibition ratios than crizotinb and ceritinib, among which four compounds (**001-017**, **002-007**, **002-008**, and **002-011**) display >50% inhibitory potency. Meanwhile, the antiproliferation activities against Karpas-299 and H3122 cell lines were also examined. As shown in Figure 2d,e, results similar to those of NCI-H2228 are observed. Compound **001-017** exhibits higher potency than **002-008** in both cells. It is not surprising that the cellular activity of **001-017** is the best among all the tested compounds since the enzyme-based IC_{50} value of **001-017** (0.27 nM) is the lowest. As a result, **001-017** emerges as a potential candidate with potent enzymatic activity against ALK and excellent antiproliferation activity in different ALK-positive cancer cell lines.

Moreover, the influence of compound **001-017** on downstream signaling pathways was also examined, and the results are illustrated in Figure 2f,g, which confirms the reduction of phospho-ALK, phospho-AKT, and phospho-STAT3 levels following **001-017** treatment. According to our results, both **001-017** and ceritinib can inhibit autophosphorylation of ALK in NCI-H2228 and Karpas-299 cell lines, and can cause substantial prevention of phosphorylation of AKT and STAT3 in a dose-dependent manner. It was also observed that compound **001-017** is more potent than ceritinib. At 10 nM, **001-017** completely suppresses ALK phosphorylation, and inhibition is observed even at 1 nM, demonstrating the unparalleled activity of **001-017** in suppressing relevant signaling pathways.

Structural Basis and Conformational Transition upon Type-I$^{1/2}$ Inhibitor Binding. The binding geometries of all the compounds were first predicted by the *Glide* docking simulations, followed by 5 ns MD simulations, and the binding free energies were subsequently calculated by the MM/GBSA methodology. Different solute dielectric constants (ε_{in} = 1, 2, and 4) were applied to get insights into the influence on the overall accuracy, which is represented by the linear correlation

DOI: 10.1021/acscentsci.7b00419
ACS Cent. Sci. 2017, 3, 1208−1220

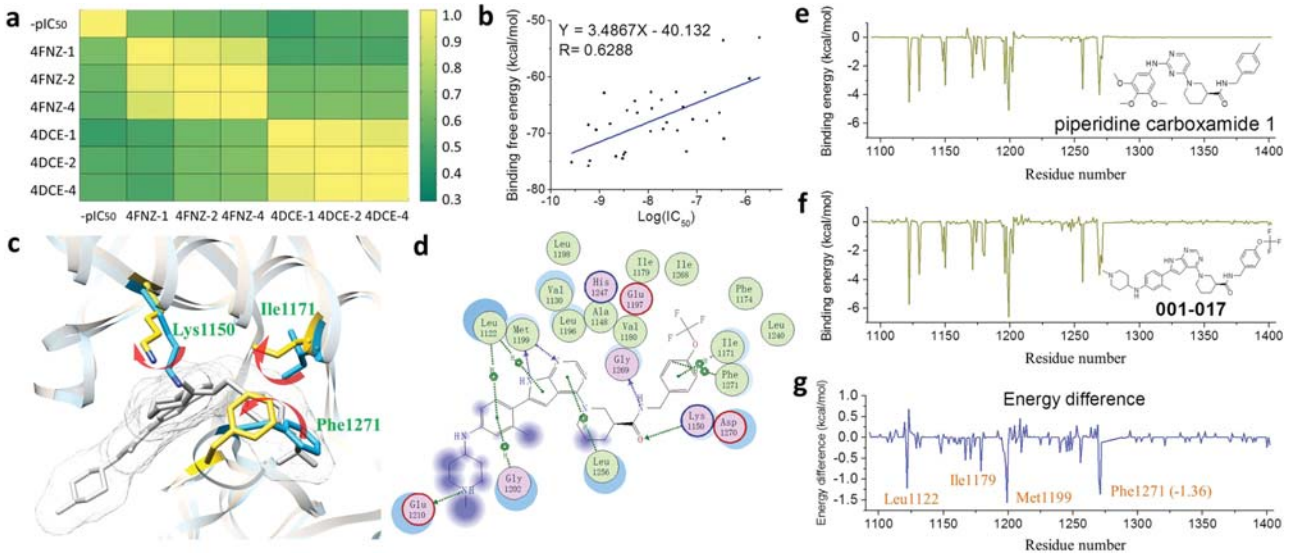

Figure 3. Molecular modeling and insights into the binding mechanism. (a) Heat map of the correlation coefficients between experimental -pIC$_{50}$ values and predicted binding free energies from six models. In order to find the best prediction model, two crystal structures of ALK (PDB entries: 4FNZ and 4DCE) were applied with the solute dielectric constants set to 1, 2, or 4 (4FNZ-1, 4FNZ-2, 4FNZ-4, 4DCE-1, 4DCE-2, and 4DCE-4). (b) Linear correlation between the predicted binding free energies and the experimental -pIC$_{50}$ values using the crystal structure of 4FNZ. The binding free energies were calculated based on the MM/GBSA methodology with the solute dielectric constant set of 1. (c) Schematic representation of the conformational shifts of the residues surrounding the hydrophobic back pocket upon the type-I$^{1/2}$ inhibitor binding. The original unbound DFG-in protein structure is shown in cyan and the DFG-shifted structure is colored in yellow. (d) 2-D schematic diagram of the binding patterns for compound **001-017**. (e, f) Protein-inhibitor interaction spectra on a per-residue basis for piperidine carboxamide 1 and compound **001-017**. The data were generated by the MM/GBSA binding free energy decomposition analysis. (g) Differences of the binding free energies ($\Delta G_{001\text{-}017} - \Delta G_{\text{piperidine carboxamide 1}}$) between piperidine carboxamide 1 and **001-017** on a per-residue basis with the important residues highlighted.

coefficient (R) between the predicted binding free energies and the experimental -pIC$_{50}$ values. Two crystal structures of ALK in complex with type-I$^{1/2}$ inhibitors (PDB codes: 4FNZ and 4DCE) were both applied in order to identify the best prediction model. As we can see in Figure 3a, the correlation coefficients are always high among the predicted binding free energies from the same crystal structure using different dielectric constants, indicating that the influence of dielectric constant on the overall prediction accuracy is limited. This result can be supported by the similar correlation coefficients between the -pIC$_{50}$ values and the predicted binding energies from each model. However, the correlation coefficients from the crystal structure of 4FNZ are slightly higher than those from 4DCE, and the correlation coefficient of the best model (4FNZ-1) can reach 0.628 (Figure 3b). So the following analyses were all carried out based on the best model of 4FNZ-1. In order to compare the performance of different approaches on the overall accuracy, we then performed MM/PBSA calculations in AMBER, prime-MM/GBSA and induced-fit docking in Schrodinger, and made a direct comparison of the performance using different methods. The linear correlation coefficients (R) between the experimental -pIC50 values and the predicted binding free energies from Glide XP docking score, induced-fit docking score, MM/GBSA (Amber), MM/PBSA (AMBER), and prime-MM/GBSA (Schrödinger) are 0.52, 0.48, 0.62, 0.65, and 0.66, respectively. It can be observed that the performance of both MM/GBSA and MM/PBSA are better than those of Glide XP docking and induced-fit docking, suggesting that MD simulation-based energy calculations display advantages in predicting the binding affinities over docking simulations. The performance of MM/PBSA is slightly better than that of MM/GBSA; however, the difference is negligible. Interestingly, the prime-MM/GBSA using single complex structure also exhibits a similar performance compared with MM/GBSA and MM/PBSA, indicating that prime-MM/GBSA could also be used as a fast rescoring method following docking simulations.

Figure 3c illustrates the conformational shifts of the residues surrounding the hydrophobic back pocket upon the binding of type-I$^{1/2}$ inhibitors. The DFG-in protein structure is shown in cyan, and the DFG-shifted structure binding to **001-017** is in yellow. Three pairs of residues that exhibit significant conformational changes upon the binding of **001-017** are highlighted as well. We can find that all the side-chains of Lys1150, Ile1171, and Phe1271 roll outward in order to accommodate the additional binding fragment. Moreover, strong hydrophobic interactions with the residues Ile1171 and Phe1271, and two hydrogen bonds with both Lys1150 and Gly1269 are formed in the extended back pocket (Figure 3d). In the ATP-binding pocket, Met1199 forms two hydrogen bonds with the nitrogen atoms of pyrrole pyrimidine, which is usually present in the binding of type-I inhibitors to ALK. The phenyl ring (R^1) connected with pyrrole pyrimidine resides in the relatively hydrophobic environment between the adenine-binding region and solvent accessible region, and forms hydrophobic contacts with both Leu1122 and Gly1202.

We further made a direct comparison between the binding features of piperidine carboxamide 1 and **001-017** in order to understand why compound **001-017** is much more potent. The binding energies on a per-residue basis were calculated based on the MM/GBSA decomposition analysis, and the differences of the binding free energies ($\Delta G_{001\text{-}017} - \Delta G_{\text{piperidine carboxamide 1}}$) were also presented. According to Figure 3e,f, both piperidine carboxamide 1 and **001-017** display similar interaction

DOI: 10.1021/acscentsci.7b00419
ACS Cent. Sci. 2017, 3, 1208−1220

behaviors, but the contribution of each residue varies. The key residues that assist the preferential binding of **001-017** to piperidine carboxamide 1 are highlighted in Figure 3g. The contributions from the residues Leu1122, Met1199, and Phe1271 are significantly higher in the binding of **001-017** to ALK. Both the hydrophobic interaction with Leu1122 and the hydrogen bonding with Met1199 in the ATP-binding region are enhanced. The dominating $\pi-\pi$ interaction with Phe1271 in the back pocket is also strengthened. These results suggest that the binding of **001-017** to both the ATP-binding site and hydrophobic back pocket is significantly stronger than that of piperidine carboxamide 1, leading to much higher overall inhibitory activity toward ALK.

Sensitivity against Drug-Resistant Mutants of ALK. The emergence of drug resistant mutants of ALK in the clinic has become a great challenge for cancer therapy. In this study, the sensitivity of compound **001-017** against four clinically resistant mutants of ALK (L1196M, C1156Y, R1275Q, and F1174L) was also evaluated, and the results are summarized in Figure 4a. L1196 M is a gatekeeper mutation, analogues to the

a

Sensitivity to ALK mutants, IC_{50} (nM)				
	L1196M	C1156Y	R1275Q	F1174L
Crizotinib	80.21	15.77	14.41	18.87
Ceritinib	9.36	12.95	6.47	10.39
001-017	7.51	4.71	2.69	9.81

b

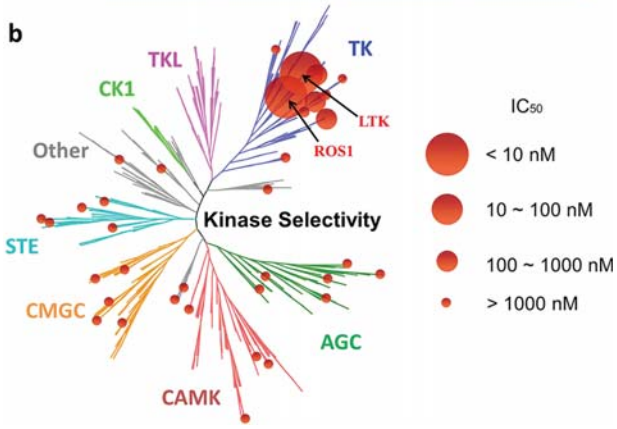

Figure 4. Sensitivity of compound **001-017** against drug-resistant mutants of ALK and selectivity toward a panel of kinases from different families. (a) Inhibitory IC_{50} values of **001-017** against four resistant ALK mutants (L1196M, C1156Y, R1275Q, and F1174L). (b) Kinase selectivity of **001-017** toward 35 kinases from different families. The size of the red circle is relevant to the value of inhibitory activity as depicted in the figure. The IC_{50} values against specific kinases are listed in Supplementary Table S2.

mutation in the EGFR-T790M kinase domain,[30] and is believed to cause resistance to the first-line drug, crizotinib. The second-generation inhibitor, ceritinib, was found to be more sensitive to the L1196M mutant. In our assays, the inhibitory IC_{50} values of crizotinib and ceritinib against L1196M ALK are 80.21 nM and 9.36 nM, respectively, consistent with the reported data. The activity of compound **001-017** (IC_{50} = 7.51 nM) against the L1196 M ALK is similar to that of ceritinib. For the C1156Y mutant, both crizotinib and ceritinib show comparable inhibitory activities (IC_{50} = 15.77 nM and 12.95 nM, respectively), but compound **001-017** is more than 3-fold more potent, with IC_{50} = 4.7 nM. In addition, compound **001-017** against the R1275Q mutant is about 7-fold more potent than crizotinib and 3-fold more potent than ceribinib. For the F1174L mutant, the sensitivities of ceritinib and **001-017** (IC_{50} = 10.39 nM and 9.81 nM, respectively) are similar, which are about 2-fold more active than that of crizotinib. In summary, compound **001-017** exhibits superior sensitivity against different genetic mutations in ALK compared with both crizotinib and ceritinib.

Kinase Selectivity. Compound **001-017** was designed as a type-$I^{1/2}$ inhibitor that binds into an extended back pocket that does not exist in most kinases. So it was expected that type-$I^{1/2}$ inhibitors would have improved kinase selectivity. To explore the kinase selectivity profile of **001-017**, the inhibitory activity on a panel of 35 kinases from different families was tested. The results are summarized in Figure 4b, and the detailed IC_{50} values against specific kinases are listed in Supplementary Table S2. Compound **001-017** shows very weak or no inhibition against most kinases. The IC_{50} values of only two kinases, LTK (0.42 nM) and ROS1 (7.88 nM), are lower than 10 nM. It is not surprising that **001-017** shows high inhibitory activity against LTK since the sequence identity between LTK and ALK is very high (~78% in the kinase domain).[31] Besides, ROS1 also shows relatively high sequence identity (~52% in the kinase domain) to ALK.[31] Apart from LTK and ROS1, none of the other kinases are found to be highly sensitive to **001-017** (>1000-fold decrease in activity), indicating that **001-017** is a highly selective ALK inhibitor.

Numerous point mutations of ALK have been identified clinically that are resistant to available therapeutic drugs. There is an urgent need to develop new inhibitors with novel chemical structures to combat drug resistance. To our knowledge, drugs currently on the market and those in clinical trials are all ATP-competitive type-I inhibitors of ALK. In this work, we designed and synthesized a series of type-$I^{1/2}$ inhibitors with very potent inhibitory activity against ALK in enzyme-based assay, with five compounds (**001-015**, **001-017**, **002-007**, **002-008**, and **002-011**) showing picomolar IC_{50}. The most potent analogue, **001-017**, is >500-fold (IC_{50} = 0.27 nM) more active than the reference compound, piperidine carboxamide 1 (IC_{50} = 174 nM), and significantly more potent than crizotinib (IC_{50} = 4.66 nM) and ceritinib (IC_{50} = 3.94 nM). On the basis of the results of structural analysis, strong hydrophobic interactions with the residues Ile1171 and Phe1271, and two hydrogen bonds with Lys1150 and Gly1269 are formed in the extended back pocket, accounting for the excellent binding affinity of **001-017**.

001-017 also shows an improved efficacy compared to both crizotinib and ceritinib against ALK-addicted cancer cells, such as NSCLC expressing EML4-ALK (NCI-H2228 and NCI-H3122) and ALCL expressing NPM-ALK (Karpas-299). We examined the influence of **001-017** on the downstream signal transduction in three cancer cell lines and confirmed the reduction of phospho-ALK, phospho-STAT3 and phospho-AKT level following the **001-017** treatment. Although the full downstream targets of the ALK signaling remain unclear, the expression of these targets can be useful markers for clinical assessment. Further investigations would be needed to clarify the exact signaling pathways of ALK and help to explore possibilities for combination therapy clinically.

To determine the potency of **001-017** to drug-resistant mutants of ALK, one of the most frequently gatekeeper mutation, L1196M, was tested first. Compound **001-017** shows high activity against the L1196M mutant. Despite a slightly

DOI: 10.1021/acscentsci.7b00419
ACS Cent. Sci. 2017, 3, 1208−1220

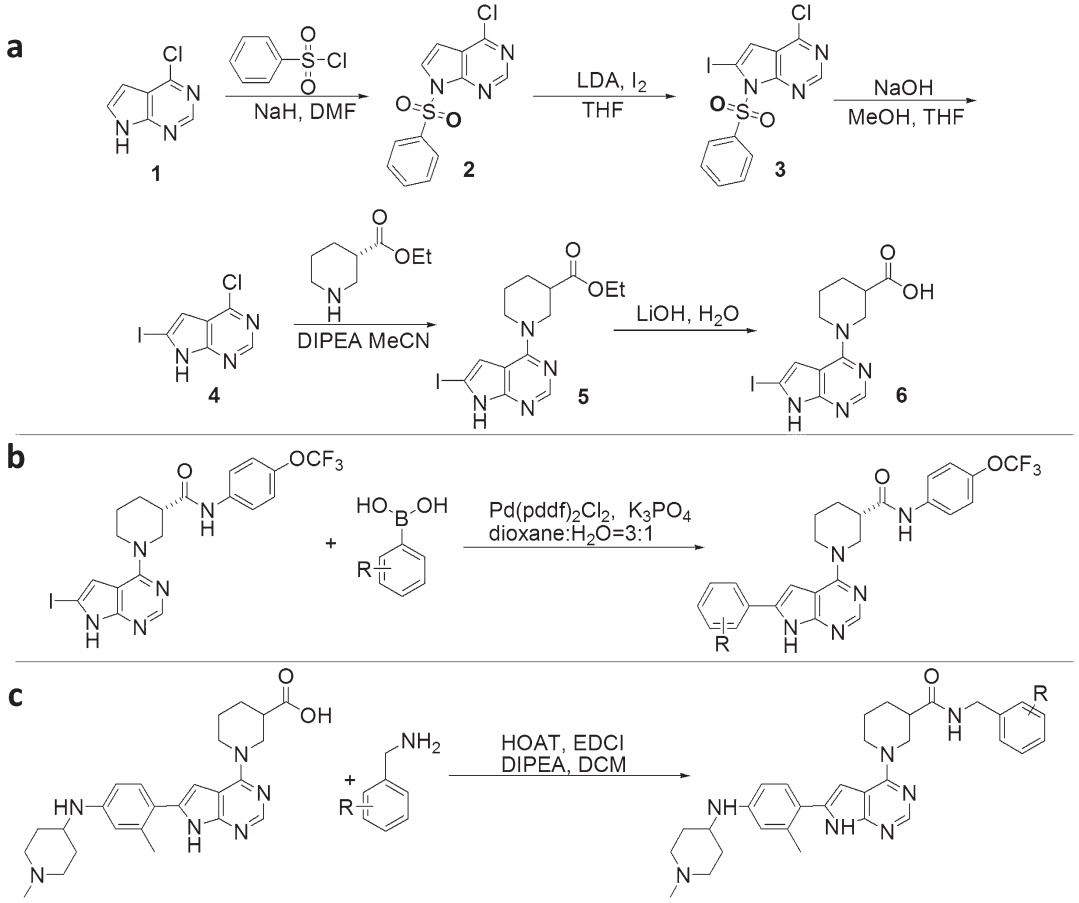

Figure 5. (a−c) General synthetic routes of 7*H*-pyrrolo[2,3-*d*]pyrimidine derivatives.

weaker binding affinity of **001-017** to the L1196M mutant compared with the native ALK, the IC_{50} value of **001-017** against this cell line is >10-fold lower than that of crizotinib. The efficacy of **001-017** against other three major resistant mutants of ALK (C1156Y, R1275Q, and F1174L) was also evaluated, and the results showed **001-017** displays superior sensitivity compared to both crizotinib and ceritinib in general.

Type-II and/or type-$I^{1/2}$ inhibitors bind into an extended hydrophobic back pocket, available to only a few kinases. Thus, the kinase selectivity of type-II and/or type-$I^{1/2}$ inhibitors is always higher than that of the ATP-competitive type-I inhibitors. In this study, the inhibitory activities of **001-017** against 35 kinases from different families were examined. Results confirm that **001-017** is a highly selective ALK inhibitor, with ∼94% kinases found immune to **001-017** (>1000-fold decrease in activity).

CONCLUSION

In conclusion, we designed a new molecular scaffold that binds to not only the ATP-binding pocket but also an extended hydrophobic back pocket, leading to very potent inhibitors against both wild-type and resistant mutants of ALK. An added benefit of this design is that the extended back pocket cannot be accessed in most kinases, therefore offering improved kinase selectivity. We expect that the inhibitors presented in this work will inspire the next generation therapy for ALK-positive cancers and provide a new strategy for developing novel ALK inhibitors to combat drug resistance.

EXPERIMENTAL SECTION

Compound Synthesis. All solvents were distilled according to general practice prior to use. All reagents were purchased and used without further purification unless specified otherwise. Solvents for flash column chromatography were technical grade and distilled prior to use. Analytical thin-layer chromatography (TLC) was performed using Huanghai silica gel plates with HSGF 254. Visualization of the developed chromatogram was performed by UV absorbance (254 nm) and appropriate stains. Flash column chromatography was performed using Qingdao Haiyang Chemical HG/T2354-92 silica gel (200−300 mesh) with the indicated solvent system according to standard techniques. ^{1}H NMR and ^{13}C NMR data were recorded on Bruker 400 MHz (100 MHz for ^{13}C, 376 MHz for ^{19}F) nuclear resonance spectrometers unless otherwise specified, respectively. Chemical shifts (δ) in ppm are reported as quoted relative to the residual signals of chloroform (^{1}H 7.26 ppm and ^{13}C 77.16 ppm). Multiplicities are described as s (singlet), bs (broad singlet), d (doublet), t (triplet), q (quartet), m (multiplet), and coupling constants (J) are reported in Hertz (Hz). ^{13}C NMR spectra were recorded with total proton decoupling.

The synthesis of compound 2 (Figure 5a): In a flamed-dried flask under Ar, NaH (3.91 g, 60% in mineral oil, 97.7 mmol) was weighed, followed by addition of DMF (150 mL). The resulting mixture was cooled to 0 °C. A solution of compound **1** (10 g, 65 mmol) in 50 mL of DMF was added slowly over a 20 min period, and the reaction solution was stirred for 30 min.

DOI: 10.1021/acscentsci.7b00419
ACS Cent. Sci. 2017, 3, 1208−1220

Benzenesulfonyl chloride (8.3 mL, 65 mmol) was added, and the mixture was warmed to r.t. and stirred for 1 h. Water was carefully added and the resulting precipitate was collected by filtration and dried in a vacuum to obtain compound **2** (17.3 g, yield: 90%) as a crystalline solid.

The synthesis of compound **3**: In a flamed-dried flask under Ar, LDA (6 mL, 2 M in THF) was added. The solution was cooled to −78 °C, and compound **2** (2,3 g, 7.83 mmol) in THF (25 mL) was added dropwise. The mixture was stirred for 1.5 h. at −78 °C, and a solution of I_2 (2.3 g, 9 mmol) in THF was added dropwise. The reaction mixture was stirred for 3 h. Water was carefully added and the mixture was extracted with three times with DCM. The organic phase was washed with brine, dried over Na_2SO_4, filtered, and concentrated to give crude product **3** (3.2 g, yield: 98%) as a yellow solid.

The synthesis of compound **4**: To a stirred solution of compound **3** (1.2 g, 2.86 mmol) in THF (15 mL) was added 5 M sodium hydroxidemethanolic solution. After 30 min, the solvent was removed under reduced pressure, and sat. NH_4Cl was added. The resulting precipitate was filtered, washed with water, and dried to afford compound **4** (783 mg, yield: 98%) as a yellow solid.

The synthesis of compound **5**: To a mixture of compound **4** (600 mg, 2.15 mmol) and ethyl (3*S*)-piperidine-3-carboxylate (406 mg, 2.58 mmol) in MeCN (30 mL) was added DIPEA (1 mL, 6.45 mmol), and the mixture was stirred at 120 °C under Ar for 48 h. The reaction mixture was cooled to r.t. and filtered to give compound **5** (629 mg, yield: 68%) as a white solid.

The synthesis of compound **6**: LiOH (1 g, 2.5 mmol) was added to a mixture of compound **5** (1 g, 2.5 mmol) in THF/H_2O = 30 mL/10 mL. The reaction solution was stirred at r.t. for 4 h. The mixture was acidified to pH = 2−3 and concentrated. Sat. $NaHCO_3$ was added until a large amount of solid precipitate appeared. The solid was collected by filtration and dried in a vacuum to obtain compound **6** (860 mg, yield: 93%).

Suzuki reaction (Figure 5b): The aryl iodide compound (100 mg, 1 equiv), 3 equiv corresponding boric acid, 0.2 equiv of $Pd(dppf)_2Cl_2$, 5 equiv of K_3PO_4 were added sequentially to a solution of dioxane/H_2O = 3 mL/1 mL. The reaction mixture was stirred under Ar at 90 °C for 15 h. The solvent was removed under a vacuum, and the residue was purified by silica gel flash column chromatography and recrystallization to afford the product.

The synthesis of the amide compound (Figure 5c): acid (100 mg, 1 equiv), 1.5 equiv of EDCI, 1.5 equiv of HOAT were added to 3 mL of DCM. The corresponding amine (1.5 equiv) and 4 equiv of DIPEA were added. The reaction mixture was stirred at r.t. overnight. Water was added and the mixture was extracted with DCM three times. The organic phase was washed with brine, dried over Na_2SO_4, filtered, and purified by silica gel flash column chromatography and recrystallization to afford product.

After the modifications of the chemical structure, 34 compounds were obtained in total, and the spectroscopic data of all the compounds can be found in the Supporting Information.

Cell-Based Antiproliferation Assay. Initially, cells were collected and seeded on 96-well plates in RPMI-1640 growth media +10% fetal bovine serum (FBS) at ∼10 000 cells/well and incubated overnight at 37 °C in 5% CO_2. The next day, serial compound dilutions were added into the assigned wells, and the plates were further cultured at 37 °C for 72 h. Cell proliferation was assessed using thiazolyl blue tetrazolium bromide (MTT) assay by adding 5 mg/mL MTT into each well, and the plates were then cultured for another 4 h. The converted dye was dissolved by MTT buffer overnight, and the absorbance of each well was finally detected at 570 nm with the control wavelength at 650 nm.

Immunoblotting Analysis. Cells were collected and lysed in cell lysis buffer (Beyotime Biotechnology, P0013) containing 1 mM PMSF and inhibitor cocktail. Cells were sonicated for 15 s to complete cell lysis and shear DNA, and the samples were then heated to 95−100 °C for 5 min. Subsequently, 20 μL samples were loaded onto sodium dodecyl sulfate-polyacrylamide gel electrophoresis (SDS-PAGE), and the proteins were then electrotransfered to polyvinylidene fluoride (PVDF) membrane (Millipore). After transfer, the membrane was washed with TBS for 5 min and incubated with blocking buffer (5% BSA) for 1 h at room temperature. Later, the membrane was incubated with diluted primary antibody (anti-ALK (Cell Signaling Technology, #3333), anti-Phospho-ALK (Cell Signaling Technology, #3341), anti-AKT (Cell Signaling Technology, #4691), anti-Phospho-AKT (Cell Signaling Technology, #4058), anti-STAT3 (Cell Signaling Technology, #4904), anti-Phospho-STAT3 (Cell Signaling Technology, #9145), and anti-GAPDH (Beyotime Biotechnology, AG019)). After further incubation with antirabbit or antimouse IgG, HRP-linked secondary antibody (Beyotime Biotechnology), the bands bound with HRP were detected using BeyoECL Plus (Beyotime Biotechnology, P0018).

Kinase Selectivity Assay. The experiments were conducted by ChemPartner Co., Ltd. CHK2 and MARK1 assays were conducted using ADP-Glo luminescent assay with ATP concentration at K_m. PI3Kα assays were also conducted by Kinase-Glo luminescent assay with ATP concentration at 25 μM. mTOR kinase assays were carried out using Lance Ultra assay with ATP concentration at K_m. The experiments of the other 31 kinases were carried out by Mobility shift assay with ATP concentration at K_m. Staurosporine or PI 103 or IKK-16 were set as the reference compound. The compounds were tested from 5 μg/mL to 0.00025 μg/mL for total of 10 concentrations (3-fold dilution). The data were fitted in XLFit to obtain IC_{50} values. Equation used is Y = bottom + (top-bottom)/(1 + (IC_{50}/X)^HillSlope).

Simulation Modeling. All docking simulations were performed using the *Glide* module in Schrödinger 9.0.[32] Preparations of the crystal structures of ALK/inhibitor complexes (PDB codes: 4FNZ and 4DCE) were carried out with the *Protein Preparation wizard* module. All crystallographic waters were removed from the original structures, and the missing hydrogen atoms and partial charges were added to the proteins. A restrained partial minimization was then performed with the maximum root-mean-square deviation (RMSD) value set to 0.3 Å. The receptor grid boxes were produced and centered on the original crystallographic inhibitors by the *Receptor gird generation* module. The scaling factors for van der Waals radii and partial atomic charge cutoff value were set to 0.8 and 0.15, respectively. Preparations of the inhibitors were all accomplished by the *LigPrep* module with protonated states generated at pH = 7.0 ± 2.0. All the other parameters were set to the default values. Finally, all the inhibitors were docked into the binding pocket of ALK using the extra precision (XP) scoring mode.

The predicted binding structures from the docking simulations served as the starting structures for molecular

DOI: 10.1021/acscentsci.7b00419
ACS Cent. Sci. 2017, 3, 1208−1220

dynamics (MD) simulations, which were all carried out using AMBER14.[33] The inhibitors were first optimized using semiempirical AM1 method in Gaussian 09,[34] and the electrostatic potential was generated at the HF/6-31G* level. The atomic partial charges were then calculated based on the RESP method by fitting the electrostatic potentials.[35] General AMBER force field (*gaff*)[36] and ff99SB force field[37] were applied to inhibitors and proteins, respectively. Each complex was immersed into a periodic TIP3P water box which was extended 8 Å from any solute atom. The Particle Mesh Ewald (PME) method was applied to handle long-range electrostatics.[38] A three-step minimization was performed before each MD simulation: (1) 1000 cycles of minimizations with 50 kcal/mol/Å^2 restraint on the backbone carbons, including 500 cycles of steepest descent and 500 cycles of conjugate gradient minimizations; (2) the same 1000 cycles of minimizations with 10 kcal/mol/Å^2 restraint; (3) 5000 cycles of minimizations without restraint, including 1000 cycles of steepest descent and 4000 cycles of conjugate gradient minimizations. Afterward, the temperature of each system was gradually elevated from 0 to 300 K in 50 ps with 2.0 kcal/mol/Å^2 restraint on the protein, and eventually 5 ns NPT (P = 1 atm and T = 300 K) MD simulations were performed with the time step set to 2 fs. The SHAKE algorithm was used to handle all hydrogen bonded atoms,[39] and the resulting MD trajectories were saved every 10 ps.

The binding free energy (ΔG_{bind}) of each inhibitor was predicted by the Molecular Mechanics/Generalized Born Solvent Area (MM/GBSA) method implemented in Amber14.[40−44] The modified Generalized Born (GB) model (*igb* = 2),[45] which has advantages over other models, was utilized to predict the polar part of desolvation energy (ΔG_{GB}), and the nonpolar part of desolvation (ΔG_{SA}) was calculated based on the solvent accessible surface area (SASA) computed by the LCPO algorithm.[46] The exterior dielectric constant was set to 80, and different solute dielectric constant (ε_{in} = 1, 2, or 4) was applied to get insights into the influence on the overall accuracy. The conformational entropic contribution ($-T\Delta S$) was not considered in the calculations due to high computational cost and low prediction accuracy.[40,47] The MM/GBSA decomposition analysis was applied to calculate the contribution of each residue to inhibitor binding.[42,48]

■ ASSOCIATED CONTENT

Supporting Information

The Supporting Information is available free of charge on the ACS Publications website at DOI: 10.1021/acscentsci.7b00419.

Antiproliferation activity of all the synthesized compounds against NCI-H2228, Karpas-299 and NCI-H3122, kinase selectivity of compound **001-017** toward 35 kinases from different families, and the NMR spectroscopic data for all the compounds (PDF)

■ AUTHOR INFORMATION

Corresponding Authors

*(T.H.) E-mail: tingjunhou@zju.edu.cn.
*(Y.H.) Email: huangyong@pkusz.edu.cn.

ORCID

Qi Liu: 0000-0001-8451-5930
Huiyong Sun: 0000-0002-7107-7481
Sunliang Cui: 0000-0001-9407-5190
Feng Zhu: 0000-0001-8069-0053
Youyong Li: 0000-0002-5248-2756
Yong Huang: 0000-0001-8377-8923
Tingjun Hou: 0000-0001-7227-2580

Notes

The authors declare no competing financial interest.

■ ACKNOWLEDGMENTS

This study was supported by the National Key R&D Program of China (2016YFA0501701; 2016YFB0201700) and the National Science Foundation of China (21575128; 81773632; 81603031). We thank the National Supercomputer Center in Guangzhou (NSCC-GZ) for providing the computing resources.

■ REFERENCES

(1) Shaw, A. T.; Kim, D. W.; Nakagawa, K.; Seto, T.; Crinó, L.; Ahn, M. J.; De Pas, T.; Besse, B.; Solomon, B. J.; Blackhall, F.; et al. Crizotinib versus chemotherapy in advanced ALK-positive lung cancer. *N. Engl. J. Med.* **2013**, *368*, 2385−2394.

(2) Shaw, A. T.; Yeap, B. Y.; Solomon, B. J.; Riely, G. J.; Gainor, J.; Engelman, J. A.; Shapiro, G. I.; Costa, D. B.; Ou, S. H. I.; Butaney, M.; et al. Effect of crizotinib on overall survival in patients with advanced non-small-cell lung cancer harbouring ALK gene rearrangement: a retrospective analysis. *Lancet Oncol.* **2011**, *12*, 1004−1012.

(3) Solomon, B. J.; Mok, T.; Kim, D. W.; Wu, Y. L.; Nakagawa, K.; Mekhail, T.; Felip, E.; Cappuzzo, F.; Paolini, J.; Usari, T.; et al. First-line crizotinib versus chemotherapy in ALK-positive lung cancer. *N. Engl. J. Med.* **2014**, *371*, 2167−2177.

(4) Shaw, A. T.; Engelman, J. A. ALK in Lung Cancer: Past, Present, and Future. *J. Clin. Oncol.* **2013**, *31*, 1105−1111.

(5) Katayama, R.; Shaw, A. T.; Khan, T. M.; Mino-Kenudson, M.; Solomon, B. J.; Halmos, B.; Jessop, N. A.; Wain, J. C.; Yeo, A. T.; Benes, C.; Drew, L.; Saeh, J. C.; Crosby, K.; Sequist, L. V.; Iafrate, A. J.; Engelman, J. A. Mechanisms of acquired crizotinib resistance in ALK-rearranged lung Cancers. *Sci. Transl. Med.* **2012**, *4*, 120ra17.

(6) Choi, Y. L.; Soda, M.; Yamashita, Y.; Ueno, T.; Takashima, J.; Nakajima, T.; Yatabe, Y.; Takeuchi, K.; Hamada, T.; Haruta, H.; Ishikawa, Y.; Kimura, H.; Mitsudomi, T.; Tanio, Y.; Mano, H. EML4-ALK Mutations in Lung Cancer That Confer Resistance to ALK Inhibitors. *N. Engl. J. Med.* **2010**, *363*, 1734−1739.

(7) Katayama, R.; Shaw, A. T.; Khan, T. M.; Mino Kenudson, M.; Solomon, B. J.; Halmos, B.; Jessop, N. A.; Wain, J. C.; Yeo, A. T.; Benes, C.; et al. Mechanisms of acquired crizotinib resistance in ALK-rearranged lung cancers. *Sci. Transl. Med.* **2012**, *4*, 120ra17.

(8) Lovly, C. M.; Pao, W. Escaping ALK inhibition: mechanisms of and strategies to overcome resistance. *Sci. Transl. Med.* **2012**, *4*, 120ps2.

(9) Sasaki, T.; Koivunen, J.; Ogino, A.; Yanagita, M.; Nikiforow, S.; Zheng, W.; Lathan, C.; Marcoux, J. P.; Du, J.; Okuda, K.; et al. A novel ALK sondary mutation and EGFR signaling cause resistance to ALK kinase inhibitors. *Cancer Res.* **2011**, *71*, 6051−6060.

(10) Sasaki, T.; Okuda, K.; Zheng, W.; Butrynski, J.; Capelletti, M.; Wang, L.; Gray, N. S.; Wilner, K.; Christensen, J. G.; Demetri, G.; et al. The neuroblastoma associated F1174L ALK mutation causes resistance to an ALK kinase inhibitor in ALK translocated cancers. *Cancer Res.* **2010**, *70*, 10038−10043.

(11) Montavon, G.; Jauquier, N.; Coulon, A.; Peuchmaur, M.; Flahaut, M.; Bourloud, K. B.; Yan, P.; Delattre, O.; Sommer, L.; Joseph, J. M.; Janoueix-Lerosey, I.; Gross, N.; Mühlethaler-Mottet, A. Wild-type ALK and activating ALK-R1275Q and ALK-F1174L mutations upregulate Myc and initiate tumor formation in murine neural crest progenitor cells. *Oncotarget* **2014**, *5*, 4452−4466.

(12) Shaw, A. T.; Kim, D. W.; Mehra, R.; Tan, D. S. W.; Felip, E.; Chow, L. Q. M.; Camidge, D. R.; Vansteenkiste, J.; Sharma, S.; Pas, T. D.; et al. Ceritinib in ALK-Rearranged Non-Small-Cell Lung Cancer. *N. Engl. J. Med.* **2014**, *370*, 1189−1197.

DOI: 10.1021/acscentsci.7b00419
ACS Cent. Sci. 2017, 3, 1208−1220

(13) Friboulet, L.; Li, N.; Katayama, R.; Lee, C. C.; Gainor, J. F.; Crystal, A. S.; Michellys, P. Y.; Awad, M. M.; Yanagitani, N.; Kim, S. The ALK inhibitor ceritinib overcomes crizotinib resistance in non-small cell lung cancer. *Cancer Discovery* **2014**, *4*, 662−673.
(14) Shaw, A. T.; Gandhi, L.; Gadgeel, S.; Riely, G. J.; Cetnar, J.; West, H.; Camidge, D. R.; Socinski, M. A.; Chiappori, A.; Mekhail, T. Alectinib in ALK -positive, crizotinib-resistant, non-small-cell lung cancer: a single-group, multicentre, phase 2 trial. *Lancet Oncol.* **2015**, *27*, 2321−2322.
(15) Ou, S. H. I.; Azada, M.; Hsiang, D. J.; Herman, J. M.; Kain, T. S.; et al. Next-Generation Sequencing Reveals a Novel NSCLC ALK F1174V Mutation and Confirms ALK G1202R Mutation Confers High-Level Resistance to Alectinib (CH5424802/RO5424802) in ALK -Rearranged NSCLC Patients Who Progressed on Crizotinib. *J. Thorac. Oncol.* **2014**, *9*, 549−553.
(16) Zou, H. Y.; Friboulet, L.; Kodack, D. P.; Engstrom, L. D.; Li, Q.; West, M.; Tang, R. W.; Wang, H.; Tsaparikos, K.; Wang, J. PF-06463922, an ALK/ROS1 Inhibitor, Overcomes Resistance to First and Second Generation ALK Inhibitors in Preclinical Models. *Proc. Natl. Acad. Sci. U. S. A.* **2015**, *28*, 1−12.
(17) Huang, W.-S.; Liu, S.; Zou, D.; Thomas, M.; Wang, Y.; Zhou, T.; Romero, J.; Kohlmann, A.; Li, F.; Qi, J.; et al. Discovery of brigatinib (AP26113), a phosphine oxide-containing, potent, orally active inhibitor of anaplastic lymphoma kinase. *J. Med. Chem.* **2016**, *59*, 4948−4964.
(18) Ahn, M.-J.; Camidge, D. R.; Tiseo, M.; Reckamp, K. L.; Hansen, K. H.; Kim, S.-W.; Huber, R. M.; West, H. J.; Groen, H. J. M.; Hochmair, M. J.; Leighl, N. B.; Gettinger, S. N.; Langer, C. J.; Paz-Ares Rodriguez, L. G.; Smit, E. F.; Kim, E. S.; Reichmann, W.; Kerstein, D.; Kim, D.-W.; Haluska, F. G. Brigatinib (BRG) in crizotinib (CRZ)-refractory ALK+ non-small cell lung cancer (NSCLC): Updates from ALTA, a pivotal randomized phase 2 trial. *J. Clin. Oncol.* **2017**, *35*, e20503−e20503.
(19) Zou, H. Y.; Friboulet, L.; Kodack, D. P.; Engstrom, L. D.; Li, Q.; West, M.; Tang, R. W.; Wang, H.; Tsaparikos, K.; Wang, J.; Timofeevski, S.; Katayama, R.; Dinh, D. M.; Lam, H.; Lam, J. L.; Yamazaki, S.; Hu, W.; Patel, B.; Bezwada, D.; Frias, R. L.; Lifshits, E.; Mahmood, S.; Gainor, J. F.; Affolter, T.; Lappin, P. B.; Gukasyan, H.; Lee, N.; Deng, S.; Jain, R. K.; Johnson, T. W.; Shaw, Alice T.; Fantin, Valeria R.; Smeal, T. PF-06463922, an ALK/ROS1 Inhibitor, Overcomes Resistance to First and Second Generation ALK Inhibitors in Preclinical Models. *Cancer Cell* **2015**, *28*, 70−81.
(20) Menichincheri, M.; Ardini, E.; Magnaghi, P.; Avanzi, N.; Banfi, P.; Bossi, R.; Buffa, L.; Canevari, G.; Ceriani, L.; Colombo, M.; Corti, L.; Donati, D.; Fasolini, M.; Felder, E.; Fiorelli, C.; Fiorentini, F.; Galvani, A.; Isacchi, A.; Borgia, A. L.; Marchionni, C.; Nesi, M.; Orrenius, C.; Panzeri, A.; Pesenti, E.; Rusconi, L.; Saccardo, M. B.; Vanotti, E.; Perrone, E.; Orsini, P. Discovery of Entrectinib: A New 3-Aminoindazole As a Potent Anaplastic Lymphoma Kinase (ALK), c-ros Oncogene 1 Kinase (ROS1), and Pan-Tropomyosin Receptor Kinases (Pan-TRKs) inhibitor. *J. Med. Chem.* **2016**, *59*, 3392−3408.
(21) Reckamp, K. L.; Infante, J. R.; Blumenschein, G. R.; Wakelee, H.; Carter, C. A.; Gockerman, J. P.; Lovly, C.; Dukart, G.; Harrow, K.; Liang, C.; Gibbons, J. J.; Horn, L. Phase I/II trial of X-396, a novel anaplastic lymphoma kinase (ALK) inhibitor, in patients with ALK+ non-small cell lung cancer (NSCLC). *J. Thorac. Oncol.* **2016**, *11*, S36−S37.
(22) Shaw, A. T.; Bauer, T. M.; Felip, E.; Besse, B.; James, L. P.; Clancy, J. S.; Mugundu, G.; Martini, J.-F.; Abbattista, A.; Solomon, B. J. Clinical activity and safety of PF-06463922 from a dose escalation study in patients with advanced ALK+ or ROS1+ NSCLC. *J. Clin. Oncol.* **2015**, *33*, 8018−8018.
(23) Drilon, A.; De Braud, F. G.; Siena, S.; Ou, S. I.; Patel, M.; Ahn, M.; Lee, J.; Bauer, T. M.; Farago, A. F.; Liu, S. V.; Reddinger, N.; Patel, R.; Luo, D.; Maneval, E. C.; Multani, P. S.; Doebele, R. C.; Shaw, A. T. Abstract CT007: Entrectinib, an oral pan-Trk, ROS1, and ALK inhibitor in TKI-naïve patients with advanced solid tumors harboring gene rearrangements: Updated phase I results. *Cancer Res.* **2016**, *76*, CT007−CT007.
(24) Horn, L.; Wakelee, H.; Blumenschein, G.; Reckamp, K.; Waqar, S.; Carter, C. A.; Gitlitz, B. J.; Infante, J. R.; Sanborn, R. E.; Neal, J.; Gockerman, J. P.; Dukart, G.; Harrow, K.; Liang, C.; Gibbons, J. J.; Hernandez, J.; Newman-Eerkes, T.; Lim, L.; Lovly, C. Phase I/II trial of X-396 in patients (pts) with ALK+ non-small cell lung cancer (NSCLC): Correlation with plasma and tissue genotyping and response to therapy (tx). *Ann. Oncol.* **2016**, *27*, 1210PD−1210PD.
(25) Davis, M. I.; Hunt, J. P.; Herrgard, S.; Ciceri, P.; Wodicka, L. M.; Pallares, G.; Hocker, M.; Treiber, D. K.; Zarrinkar, P. P. Comprehensive analysis of kinase inhibitor selectivity. *Nat. Biotechnol.* **2011**, *29*, 1046−1051.
(26) Bryan, M. C.; Whittington, D. A.; Doherty, E. M.; Falsey, J. R.; Cheng, A. C.; Emkey, R.; Brake, R. L.; Lewis, R. T. Rapid development of piperidine carboxamides as potent and selective anaplastic lymphoma kinase inhibitors. *J. Med. Chem.* **2012**, *55*, 1698−1705.
(27) Tu, C.; Lin, W.; Peng, Y.; Hsu, T.; Wu, J.; Chang, C.; Lu, C.; Lyu, P.; Shih, C.; Jiaang, W.; Wu, S. Pyrazolylamine Derivatives Reveal the Conformational Switching between Type I and Type II Binding Modes of Anaplastic Lymphoma Kinase (ALK). *J. Med. Chem.* **2016**, *59*, 3906−3919.
(28) Zuccotto, F.; Ardini, E.; Casale, E.; Angiolini, M. Through the "gatekeeper door": exploiting the active kinase conformation. *J. Med. Chem.* **2010**, *53*, 2681−2694.
(29) Kong, X.; Pan, P.; Li, D.; Tian, S.; Li, Y.; Hou, T. Importance of protein flexibility in ranking inhibitor affinities: modeling the binding mechanisms of piperidine carboxamides as Type I1/2 ALK inhibitors. *Phys. Chem. Chem. Phys.* **2015**, *17*, 6098−6113.
(30) Giroux, S. Overcoming acquired resistance to kinase inhibition: the cases of EGFR, ALK and BRAF. *Bioorg. Med. Chem. Lett.* **2013**, *23*, 394−401.
(31) Iwahara, T.; Fujimoto, J.; Wen, D.; Cupples, R.; Bucay, N.; Arakawa, T.; Mori, S.; Ratzkin, B.; Yamamoto, T. Molecular characterization of ALK, a receptor tyrosine kinase expressed specifically in the nervous system. *Oncogene* **1997**, *14*, 439−449.
(32) *Schrödinger*, Version 9.0; Schrödinger LLC: New York, NY, 2009.
(33) Case, D.; Babin, V.; Berryman, J.; Betz, R.; Cai, Q.; Cerutti, D.; Cheatham, T., III; Darden, T.; Duke, R.; Gohlke, H. *AMBER 14*; University of California: San Francisco, 2014.
(34) Frisch, M. J.; Trucks, G.; Schlegel, H.; Scuseria, G.; Robb, M.; Cheeseman, J.; Scalmani, G.; Barone, V.; Mennucci, B.; Petersson, G. *Gaussian 09*; Gaussian Inc.: Wallingford, CT, 2009.
(35) Bayly, C. I.; Cieplak, P.; Cornell, W.; Kollman, P. A. A well-behaved electrostatic potential based method using charge restraints for deriving atomic charges: the RESP model. *J. Phys. Chem.* **1993**, *97*, 10269−10280.
(36) Wang, J. M.; Wolf, R. M.; Caldwell, J. W.; Kollman, P. A.; Case, D. A. Development and testing of a general amber force field. *J. Comput. Chem.* **2004**, *25*, 1157−1174.
(37) Duan, Y.; Wu, C.; Chowdhury, S.; Lee, M. C.; Xiong, G. M.; Zhang, W.; Yang, R.; Cieplak, P.; Luo, R.; Lee, T.; Caldwell, J.; Wang, J. M.; Kollman, P. A point-charge force field for molecular mechanics simulations of proteins based on condensed-phase quantum mechanical calculations. *J. Comput. Chem.* **2003**, *24*, 1999−2012.
(38) Darden, T.; York, D.; Pedersen, L. Particle mesh Ewald: An W log (N) method for Ewald sums in large systems. *J. Chem. Phys.* **1993**, *98*, 10089−10092.
(39) Ryckaert, J. P.; Ciccotti, G.; Berendsen, H. J. C. Numerical integration of the cartesian equations of motion of a system with constraints: molecular dynamics of n-alkanes. *J. Comput. Phys.* **1977**, *23*, 327−341.
(40) Wang, J.; Wang, W.; Kollman, P. A.; Case, D. A. Automatic atom type and bond type perception in molecular mechanical calculations. *J. Mol. Graphics Modell.* **2006**, *25*, 247−260.
(41) Kollman, P. A.; Massova, I.; Reyes, C.; Kuhn, B.; Huo, S.; Chong, L.; Lee, M.; Lee, T.; Duan, Y.; Wang, W.; et al. Calculating structures and free energies of complex molecules: combining molecular mechanics and continuum models. *Acc. Chem. Res.* **2000**, *33*, 889−897.

DOI: 10.1021/acscentsci.7b00419
ACS Cent. Sci. 2017, 3, 1208−1220

(42) Hou, T.; Li, N.; Li, Y.; Wang, W. Characterization of Domain-peptide Interaction Interface: Prediction of SH3 Domain-Mediated Protein-protein Interaction Network in Yeast by Generic Structure-Based Models. *J. Proteome Res.* **2012**, *11*, 2982−2995.
(43) Hou, T.; Zhang, W.; Case, D. A.; Wang, W. Characterization of domain-peptide interaction interface: A case study on the amphiphysin-1 SH3 domain. *J. Mol. Biol.* **2008**, *376*, 1201−1214.
(44) Hou, T. J.; Xu, Z.; Zhang, W.; McLaughlin, W. A.; Case, D. A.; Xu, Y.; Wang, W. Characterization of Domain-Peptide Interaction Interface. *Mol. Cell. Proteomics* **2009**, *8*, 639−649.
(45) Onufriev, A.; Bashford, D.; Case, D. A. Exploring protein native states and large-scale conformational changes with a modified generalized born model. *Proteins: Struct., Funct., Genet.* **2004**, *55*, 383−394.
(46) Weiser, J.; Shenkin, P. S.; Still, W. C. Approximate atomic surfaces from linear combinations of pairwise overlaps (LCPO). *J. Comput. Chem.* **1999**, *20*, 217−230.
(47) Hou, T. J.; Li, Y. Y.; Wang, W. Prediction of peptides binding to the PKA RII alpha subunit using a hierarchical strategy. *Bioinformatics* **2011**, *27*, 1814−1821.
(48) Gohlke, H.; Kiel, C.; Case, D. A. Insights into protein-protein binding by binding free energy calculation and free energy decomposition for the Ras-Raf and Ras-RalGDS complexes. *J. Mol. Biol.* **2003**, *330*, 891−914.

DOI: 10.1021/acscentsci.7b00419
ACS Cent. Sci. 2017, 3, 1208−1220